in vivo *36*: 2149-2165 (2022)
doi:10.21873/invivo.12941

In Vivo Analysis of the Immune Response to Strontium- and Copper-doped Bioglass

MIKE BARBECK[1,2], SAID ALKILDANI[1,2], ARMANDO MANDLULE[3], MILENA RADENKOVIĆ[4], STEVO NAJMAN[4,5], SANJA STOJANOVIĆ[4,5], OLE JUNG[1], YANRU REN[1,6], BAOYI CAI[1,6], OLIVER GÖRKE[3], DENIS RIMASHEVSKIY[6*] and FRANZISKA SCHMIDT[7,8*]

[1]*Clinic and Policlinic for Dermatology and Venereology, University Medical Center Rostock, Rostock, Germany;*
[2]*BerlinAnalytix GmbH, Berlin, Germany;*
[3]*Department of Ceramic Materials, Institute for Materials Science and Technologies, Technical University of Berlin, Berlin, Germany;*
[4]*Department for Cell and Tissue Engineering, Faculty of Medicine, University of Niš, Niš, Serbia;*
[5]*Department of Biology and Human Genetics, Faculty of Medicine, University of Niš, Niš, Serbia;*
[6]*Department of Traumatology and Orthopedics, Peoples' Friendship University of Russia, Moscow, Russia;*
[7]*Department of Prosthodontics, Geriatric Dentistry and Craniomandibular Disorders, Charité-Universitätsmedizin Berlin, Corporate Member of Freie Universität Berlin, Humboldt-Universität zu Berlin, Berlin, Germany*
[8]*Berlin Institute of Health, Berlin, Germany*

Abstract. *Background: Bioglass is a highly adoptable bone substitute material which can be combined with so-called therapeutic ions. However, knowledge is poor regarding the influence of therapeutic ions on immune reactions and associated bone healing. Thus, the aim of this work was to investigate the influence of strontium- and copper-doped bioglass on the induction of M1 and M2 macrophages, as well as vascularization. Materials and Methods: Two types of alkali glass were produced based on ICIE16 bioglass via the melt-quench method with the addition of 5 wt% copper or strontium (ICIE16-Cu and ICIE16-Sr). Pure ICIE16 and 45S5 bioglass were used as control materials. The ion release and chemical composition of the bioglass were investigated, and an in vivo experiment was subcutaneously performed on Sprague–Dawley rats. Results: Scanning electron microscopy revealed significant differences in the surface morphology of the bioglass materials. Energy dispersive X-ray spectroscopy confirmed the efficiency of the doping process by showing the ion-release kinetics. ICIE16-Cu exhibited a higher ion release than ICIE16-Sr. ICIE16-Cu induced low immune cell migration and triggered not only a low number of M1 and M2 macrophages but also of blood vessels. ICIE16-Sr induced higher numbers of M1 macrophages after 30 days. Both bioglass types induced numbers of M2 macrophages comparable with those found in the control groups. Conclusion: Bioglass doping with copper and strontium did not significantly influence the foreign body response nor vascularization of the implantation bed in vivo. However, all the studied bioglass materials seemed to be biocompatible.*

*These Authors contributed equally to this study.

Correspondence to: Mike Barbeck, Clinic and Policlinic for Dermatology and Venereology, University Medical Center Rostock, 18057 Rostock, Germany. Tel: +49 17681022467, e-mail: mike.barbeck@med.uni-rostock.de

Key Words: Bioglass, ion release, hydroxyapatite deposition, bone tissue regeneration, macrophages, vascularization, copper doping, strontium doping, 45S5, ICIE16, DIN EN ISO 10993-6.

Bone substitute materials (BSMs) are a small group including biomaterials mainly based on natural or synthetic calcium phosphates and similar compounds (1). Bioactive glass is a specific subgroup which has been shown to be a good BSM due to its optimal bonding to newly formed bone tissue and due to the formation of a hydroxycarbonate apatite layer which supports bone regeneration (2). Since the invention of bioactive glass materials in the 1970s by Professor Larry L. Hench, with 45S5® bioglass being one of the first developed materials, much research has been conducted on bioactive glass (3). Silicate-based bioactive glass and glass ceramics, such as Perioglas® (4) and Ceravital® (5, 6), have been clinically used as BSMs for several decades. Nevertheless,

45S5® has some disadvantages, such as the small processing window, which can lead to crystallization during the production process and thus to a reduction of bioactivity due to the presence of crystalline and amorphous phases (7, 8). Furthermore, the original composition includes a large amount of sodium to reduce the melting temperature (9), which leads to cell death under *in vitro* conditions due to a burst release and subsequent fast increase in pH (10). Because of its high crystallization tendency, 45S5 is difficult to shape it into glass fibers or amorphous scaffolds without changing its initial properties and thus its ability to bond to bone. In contrast, ICIE16 (by weight 48.0% SiO_2, 6.6% Na_2O_3, 2.9% CaO, 2.5% P_2O_5, 10.0% K_2O) was developed by Elgayar and co-workers (11). It has a lower tendency to crystallize and a greater sintering window (12), which makes it a promising agent for producing various shapes, including amorphous scaffolds (13).

One of the most worthwhile features of bioactive glass is the ability to incorporate vast quantities of additives into them, such as therapeutic ions (*e.g.*, strontium, copper, zinc, or fluorine) or drugs (14). In this context, ICIE16 is an ideal candidate for incorporation of therapeutically active ions into scaffolds, which can be used for controlled degradation (13, 15). Therapeutic ions can be added in the form of metallic ions and are also naturally present in the body. Although they occur in the body at lower concentrations in the form of trace elements (16), higher quantities released from bioactive glass have stimulatory effects on certain cells, without being toxic (16-18). Thus, therapeutic ions are able to enhance the biological impact of bioactive glass and, therefore, strengthen bone formation due to their stimulating effects (19). Like any other biomaterial, bioactive glass induces an inflammatory reaction within their implant bed (16, 20). This reaction cascade, also known as the 'foreign body reaction to biomaterials' includes macrophages as central control elements, which significantly control material-specific inflammation through the expression of a variety of signaling molecules (21). The consensus is that a biomaterial should induce an anti-inflammatory tissue response, and thereby also a predominance of M2 macrophages, in order to support tissue regeneration optimally (22). The addition of strontium leads to stimulation of osteoblasts and reduction of osteoclast activity (19, 23). Its inclusion induces new bone formation, and it is therefore widely used as a therapeutic ion for osteoporosis (24). Furthermore, copper is known for its promotion of angiogenesis and (related) stimulation of bone regeneration (25, 26). However, it is completely unknown what influence these so-called therapeutic ions have on inflammatory tissue reactions that are strongly connected with tissue regeneration (16, 19). Thus, it was supposed that their inclusion might be used to control the material-triggered healing process by regulating the induction of M2 macrophages. In this context, it was shown that copper, zinc, and silver have anti-inflammatory and antimicrobial properties (27). The use of therapeutic ions in dental applications may therefore provide advantages compared to both purely inorganic calcium phosphate-based bone substitute materials and to organic biomolecules (*e.g.*, growth factors). Altogether, the addition of therapeutic ions to bioactive glass might be expected to lead to a better bone-healing process by adaption of the associated and underlying inflammatory reactions.

Thus, the aim of this work was to investigate the influence of the release of strontium and copper ions from bioactive glass-based BSM on the induction of M1 and M2 macrophage subtypes.

The objectives of the present study were: (a) The synthesis of bioactive glass 45S5 (by weight: 45% SiO_2, 24.5% CaO, 24.5% Na_2O, and 6.0% P_2O_5) and ICIE16 (by weight: 48.0% SiO_2, 6.6% Na_2O, 32.9% CaO, 2.5% P_2O_5, 10.0% K_2O); (b) incorporation of 5 mol% strontium or copper ions into ICIE16; (c) examination of the influence of strontium and copper on the resulting structure and material properties; (d) evaluation of the influence of strontium and copper on the bioactivity of the synthesized glass and the ability to form a hydroxycarbonate apatite layer; (e) assessment of inflammatory tissue reaction induced by ICIE16 and the strontium- and copper-doped glass after subcutaneous implantation for 10 and 30 days using previously established and published methodologies (14, 28, 29). Thereby, both pure ICIE16 and 45S5 bioglass implants served as control materials. 45S5 Bioglass was used as a control due to its proven biocompatibility in literature (14).

Materials and Methods

Materials. Four different bioglass alkali systems were synthesized by melt quenching, namely 45S5 (by weight: 45% SiO_2, 24.5% CaO, 24.5% Na_2O, and 6.0% P_2O_5), ICIE16 (by weight: 48.0% SiO_2, 6.6% Na_2O, 32.9% CaO, 2.5% P_2O_5, 10.0% K_2O), 5 mol% Cu-doped (ICIE16-Cu) and 5 mol% Sr-doped (ICIE16-Sr) ICIE16. 45S5 and ICIE16 were prepared as control materials. Compared to 45S5, ICIE16 has a lower crystallization tendency during sintering and remains amorphous up to 700˚C (30). Table I provides the molecular composition of each bioglass.

Per batch, 100 g of bioglass were prepared *via* a melt-quench process. High-purity powders [SiO_2, Na_2CO, $Ca_5HO_{13}P_3$, $Ca(OH)_2$, K_2CO_3, $CuCO_3$, and $SrCO_3$] were weighed out according to the desired relative ratios, dried at 100˚C for 24 h, melted at 1,400˚C for 2 h, quenched at room temperature after 2 h, dried at 100˚C overnight, milled to 100-315 μm particle size for 3 min *via* dry ball-milling, and finally pressed into pellets (diameter: 1 mm, height: 0.5 mm) using pressure of 15 bars for 3 min. Finally, the materials underwent gamma-sterilization.

Bioglass characterization. *In vitro:* The surface morphology of the prepared bioglass materials was characterized *via* scanning electron microscopy (SEM) with a LEO Gemini 1530 SEM (Carl Zeiss SMT GmbH, Oberkochen, Germany) after preparation by means of a

Table I. *Nominal composition of the investigated bioglass types (mol%).*

Material		SiO_2	P_2O_5	Na_2O	CaO	K_2O	CuO	SrO
Control	45S5	46.1	2.6	24.4	26.9	0	0	0
	ICIE16	49.46	1.07	6.6	36.27	6.6	0	0
Test	ICIE16-Cu	46.99	1.02	6.27	34.46	6.27	5	0
	ICIE16-Sr	46.99	1.02	6.27	34.46	6.27	0	5

washing step with ethanol and drying at 50˚C. The samples were then carbon- and gold-sputtered and examined at accelerating voltages of 10-20 kV. Furthermore, energy-dispersive X-ray (EDX) spectra (Kα line) of disc surface areas of 1×1 μm^2 were recorded at 10 and 20 kV in field emission gun SEM to analyze the chemical composition and level of contamination qualitatively.

Inductively coupled plasma optical emission spectrometry (ICP-OES): The simulated body fluid (SBF) was prepared according to Kokubo *et al*. (31). The bioglass samples were immersed in the SBF and incubated at 37˚C for 3, 7, and 14 days, under static conditions. After incubation, the samples were removed, and ICP-OES measurements were performed using Ultima-2 (Horiba, Kyoto, Japan) at 252.851 nm to determine the amounts of ions which were dissolved from the bioglass samples into the SBF. For each sample, three measurements were conducted at days 3, 7, and 14.

In vivo study. Experimental design. Subcutaneous implantation was performed on 32 female Sprague–Dawley rats, 3 to 4 months old, weighing 255±15 g, (Military Medical Academy, Belgrade, Serbia) that were randomly assigned to groups according to bioglass type and time point (n=4 per each group and time point). The experimental animals were anesthetized *via* an intraperitoneal injection of ketamine (100 mg/kg of body weight) and xylazine (5 mg/kg of body weight). A midline incision was made in the skin of the scapular region, followed by a blunt incision to create a subcutaneous pocket. Then 100 mg of bioglass was implanted in the subcutaneous pocket under sterile conditions and the wound was stitched with nonabsorbable suture materials. At 10 or 30 days post implantation, animals were sacrificed using an overdose of the anesthesia to analyze both the early and late tissue responses to the biomaterials in accordance with previous publications (28, 32). The biomaterials were extracted with their surrounding tissue and placed in formaldehyde solution for preservation for 24 h. Experiments were authorized by the Local Ethical Committee of the Faculty of Medicine (University of Niš, Serbia) based on the approval of the Veterinary Directorate of the Ministry of Agriculture, Forestry and Water Management of the Republic of Serbia (approval number 323-07-01762/2019-05/9; date of approval: 01 March 2019).

Histological workup. The explants were processed with an initial dehydration through increasing ethanol concentrations and cleared in xylene. Afterwards, the explants were treated with 10% Tris-buffered ethylenediaminetetraacetic acid for 2 weeks for decalcification to allow subsequent sectioning. The explants were then embedded in paraffin. The paraffin blocks were sectioned at 3-5 μm thickness. Serial sections were used for histochemical staining (*i.e*., hematoxylin and eosin) and immunohistochemical staining, *i.e*., against CD11c for detection of M1 macrophages, CD163 for detection of M2 macrophages, and CD31 for detection of endothelial cells). All antibodies were obtained from Abcam (Cambridge, UK). Immunohistochemical staining has been thoroughly described by Lindner *et al*. (28). In brief, the histological sections were treated with citrate buffer and proteinase K at pH 8 for 20 min in a water bath at 96˚C, followed by equilibration using TBS-T buffer. Subsequently, the slides were prepared by H2O2 and avidin and biotin blocking solutions (Avidin/Biotin Blocking Kit; Vector Laboratories, Burlingame, CA, USA). Incubation with the respective primary antibody for 30 min was conducted, followed by incubation with the secondary antibody (goat anti-rabbit IgG-B, sc-2040, 1:200; Santa Cruz Biotechnology, Shandon, CA, USA). Afterward, the avidin–biotin–peroxidase complex (ThermoFisher Scientific, Dreeich, Germany) was applied for 30 min, and counterstaining by bluing was conducted.

Histological and histomorphometrical analysis. Histopathological evaluation was conducted using a conventional diagnostic microscope (Axio Imager M2; Zeiss, Oberkochen, Germany). The evaluation included determining the state of the implantation bed and biomaterial, by assessment of granulation tissue, types of immune cells [granulocytes, lymphocytes, macrophages, and biomaterial-associated multinucleated giant cells (BMGCs)], vascularization, fibrosis, hemorrhage, and necrosis. Photographs were taken using an Axiocam 506 color connected to its software ZEN Core (Zeiss).

To conduct the quantitative histomorphometrical analysis, the immunohistochemically stained slides were initially digitized using a scanning microscope (M8; PreciPoint GmbH, Munich, Germany). The frequency of M1 and M2 macrophages was analyzed using a plugin in ImageJ (National Institutes of Health, Bethesda, MA, USA) that was developed by Lindner and colleagues (28). This plugin allows measurement of the number of positively stained cells per mm^2 and the vascularization pattern (vessels/mm^2 and percentage vascularization).

Evaluation of the local biological effects of bioglass implantation based on semiquantitative histopathological scoring. Histopathological scoring of the local effects of bioglass implantation was conducted based on ISO 10993:2016, Part 6, Annex E (33). All microscopic analysis was performed by a single experienced pathologist who was blinded through coded slides. A semiquantitative histological analysis was performed on each slide from which six high-power fields (×400) were scanned according to the area of interest, without any overlap, establishing a count of the surveyed cells and resulting in a score value indicating predominance among them. The biological response parameters at the bioglass interface were evaluated and irritancy/reactivity was scored as shown in Table II. The mean and the standard deviation of the scoring results of the six visual fields were calculated for each test material

Table II. *Histological evaluation system for irritancy/reactivity—cell type/response. The overall irritancy score was calculated using the individual component scores: (polymorphonuclear cells+lymphocytes+plasma cells+macrophages+giant cells+necrosis)×2+(neovascularization+fibrosis+fatty infiltrate).*

	Component score				
Response	0	1	2	3	4
Polymorphonuclear cells	0	Rare, 1-5/hpf	6-10/hpf	Heavy infiltrate	Packed
Lymphocytes	0	Rare, 1-5/hpf	6-10/hpf	Heavy infiltrate	Packed
Plasma cells	0	Rare, 1-5/hpf	6-10/hpf	Heavy infiltrate	Packed
Macrophages	0	Rare, 1-5/hpf	6-10/hpf	Heavy infiltrate	Packed
Giant cells	0	Rare, 1-2/hpf	3-5/hpf	Heavy infiltrate	Packed
Necrosis/osteolysis	0	Minimal	Mild	Moderate	Marked
Neovascularization	0	Minimal capillary proliferation focal, 1-3 buds	Groups of 4-7 capillaries with supporting fibroblastic structures	Broad band of capillaries with supporting structures	Extensive band of capillaries with supporting fibroblastic structures
Fibrocytes/fibroconnective tissue, fibrosis	0	Narrow band	Moderately thick band	Thick band	Extensive band
Fatty infiltrate	0	Minimal amount of fat associated with fibrosis	Several layers of fat and fibrosis	Elongated and broad accumulation of fat cells about the implant site	Extensive fat completely surrounding the implant

Hpf: High-powered field (×400).

and the control material (45S5 bioglass). Finally, according to Annex E, Table E of DIN EN ISO 10993-6:2016 (33), for each test material the relative irritancy was calculated as: Irritancy score of the test material −irritancy score of the control material, while a negative difference was assigned a score of 0. Irritancy status was assigned according to the values listed in Table III.

Statistical analysis. Quantitative data from the histomorphometrical analysis are presented as means with standard deviation. The data were analyzed using analysis of variance tool *via* GraphPad Prism 9.3.1 software (GraphPad Inc., La Jolla, CA, USA). Statistical differences were designated as significant when *p*-values were less than 0.05. Both inter and intra-individual significances were calculated.

Results

Bioglass characterization. SEM analysis. The analysis *via* SEM revealed significant differences in the surface morphology of the (Figure 1). The surface morphology ranged from an almost smooth surface of the 45S5 bioglass to predominantly crystalline surface structures of ICIE16 and ICIE16-Sr, to a vesicular surface pattern in the case of ICIE16-Cu (Figure 1).

EDX spectroscopy. EDX spectroscopy was used to determine the qualitative chemical composition of the samples. EDX analyses revealed the presence of Si, Na, Ca, P, and O in the 45S5 samples, as well as of additional K in ICIE16 samples (Figure 2). Moreover, it confirmed the presence of Cu and Sr in the ion-doped ICIE16 bioglass materials (Figure 2).

Table III. *Irritancy/reactivity grade [adapted from DIN EN ISO 10993-6 (33)].*

Overall irritancy score	Irritancy/reactivity status
0.0 to 2.9	Minimal or no reaction (non-irritant)
3.0 to 8.9	Slight reaction (slight irritant)
9.0 to 15.0	Moderate reaction (moderate irritant)
>15.1	Severe reaction (severe irritant)

ICP-OES. The release of ions from the ICIE16-Cu and ICIE16-Sr materials was measured before and after immersion in SBF for 3, 7, and 14 days (Figure 3). The release of both ions consistently significantly increased with time ($p<0.001$) (Figure 3). Moreover, a significantly higher copper release was found at every time point compared to strontium (Figure 3).

In vivo histopathological analysis. Histological analysis showed that the different types of bioglass were detectable within the subcutaneous connective tissue at day 10 and 30 post implantation. Moreover, no tissue ingrowth into the bioglass pellets was detected. All bioglass materials were surrounded by inflammatory cell types, *i.e.*, mainly macrophages, as well as lower numbers of granulocytes and fibroblasts at 10 days post implantation (Figure 4). Furthermore, single multinucleated giant cells (BMGCs) were detectable at the material surfaces in all study groups. The histopathological analysis revealed comparable extents

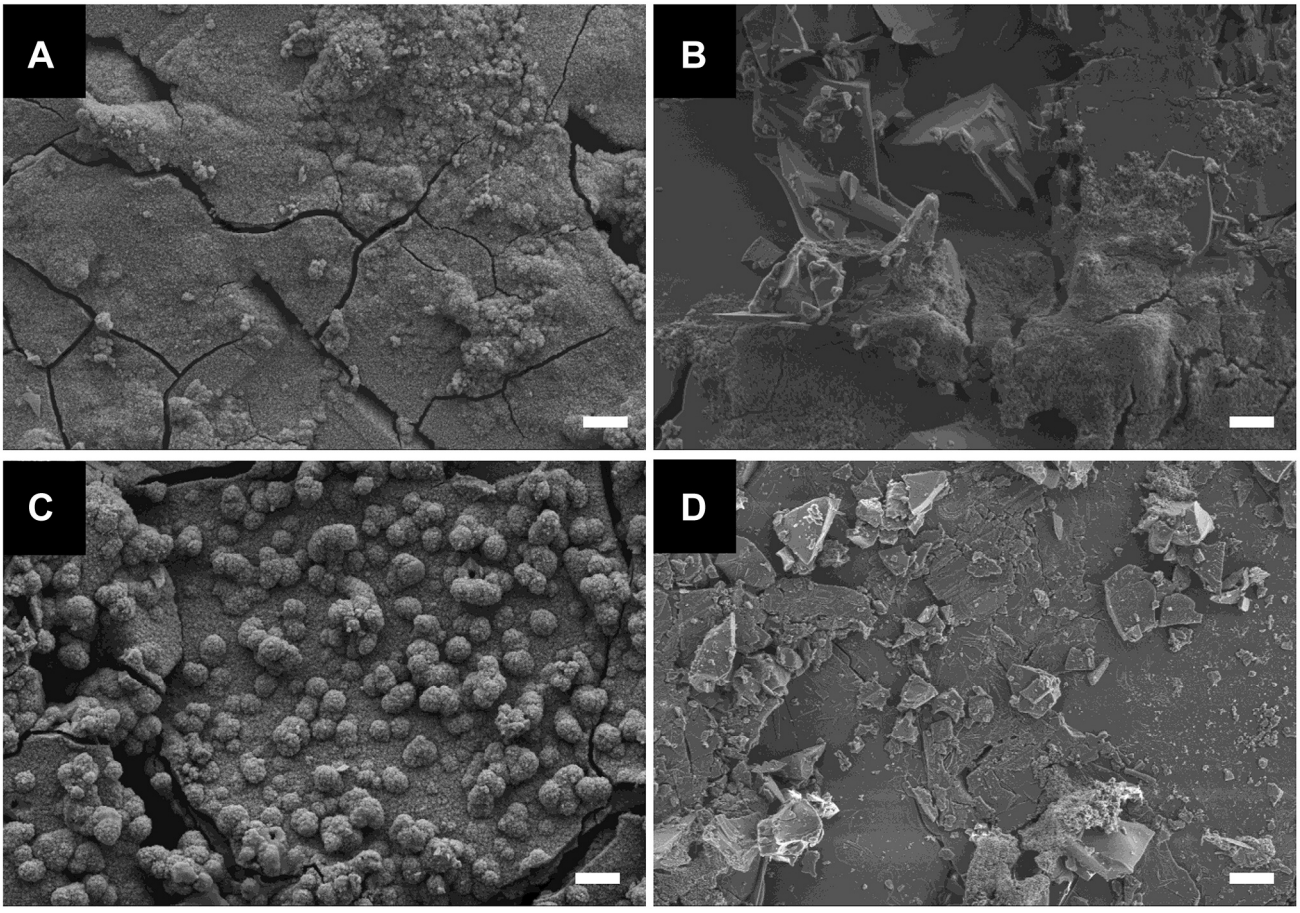

Figure 1. *Exemplary scanning electron microscopy images of the surface morphology in 45S5 (A), ICIE16 (B), ICIE16-Sr (C) and ICIE16-Cu (D) bioglass (200× magnification; scale bars=10 μm).*

of inflammatory tissue reactions in all four study groups. However, immunohistochemical detection revealed fewer macrophages within the implantation beds of animals receiving ICIE16-Cu bioglass and especially lower numbers of CD163-positive macrophages in this group compared to the other groups (Figure 5). Between the three other study groups, no visible differences in the occurrence of CD163-positive cells were observed. Moreover, the analysis showed that minimally lower numbers of CD11c-positive macrophages were observed in the ICIE16-Cu bioglass group compared to the other study groups. No differences in the occurrence of this macrophage subtype ware observed in the other study groups (Figure 6). Additionally, visibly lower numbers of pro-inflammatory macrophages were observable in all study groups. Furthermore, comparable numbers of small vessels were found within the reactive connective tissue neighboring each implant (Figure 7).

At day 30 post implantation, still comparable tissue reaction patterns were detected in all groups. Histopathological analyses showed that the same types of cells, *i.e.*, mainly macrophages, as well as single granulocytes and fibroblasts were involved (Figure 8). However, the number of BMGCs at the material surface was slightly increased in all groups. Additionally, the histopathological analyses revealed that the numbers of M1 macrophages had visibly increased in the groups with CIE16-Sr and the pure ICIE16 bioglass and their numbers were higher compared to the number of CD163-positive M2 macrophages. In contrast, in the ICIE16-Cu and 45S5 bioglass groups, comparative numbers of both macrophage subtypes were observed (Figure 5 and Figure 6). The observation of the implantation bed vascularization showed that comparable numbers of vessels were still apparent within the granulation and connective tissues surrounding all bioglass materials (Figure 7).

Results of the histopathological scoring. Histopathological scoring resulted in similar inflammation in all groups at day 10 post implantation (Table IV). The inflammatory tissue response to the bioglass included cells of the immune system, *i.e.*, mainly polymorphonuclear cells/granulocytes (moderate presence),

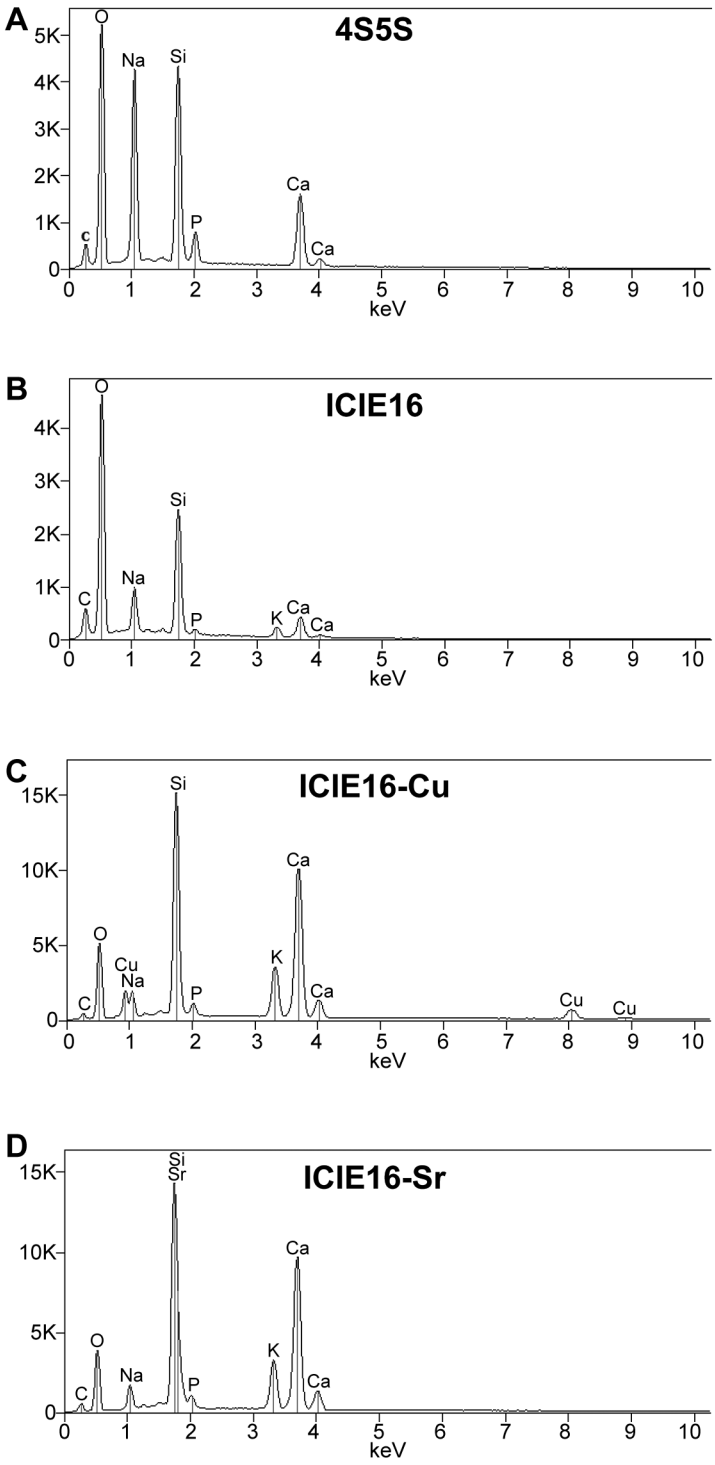

Figure 2. *Energy-dispersive X-ray spectroscopy spectra of the 45S5 (A), ICIE16 (B), ICIE16-Cu (C) and ICIE16-Sr (D) bioglass materials.*

lymphocytes (moderate presence), plasma cells (rare), macrophages (moderate presence) and giant cells (moderate presence), which were comparable in all groups, as was neovascularization (moderate); whereas fibrosis was moderate in all ICIE16 groups and, rare in the 45S5 group). Fatty infiltrate was not detectable in any group, nor was necrosis.

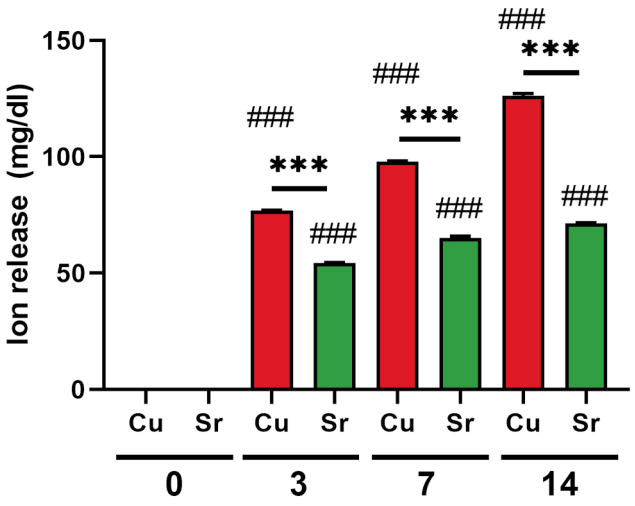

Figure 3. *Release of Cu ions from ion-doped ICIE16-Cu and Sr ions from ICIE-16-Sr bioglass materials after immersion in simulated body fluid (SBF) for 3, 7, and 14 days. Significantly different at p<0.001: ***between metals; ###between bioglass samples of the same type.*

Histopathological scoring resulted in comparable degrees of inflammation at day 30 post implantation (Table IV). The inflammatory tissue response to the bioglass included cells of the immune system, *i.e.* mainly polymorphonuclear cells/granulocytes (moderate presence, comparable in all groups), lymphocytes (moderate presence, comparable in all groups), plasma cells (rare presence, comparable in all groups), macrophages (moderate presence, comparable in all groups), giant cells (moderate presence, comparable in all groups), neovascularization (moderate, comparable in all groups), fibrosis (moderate in the groups of the ICIE16 bioglass, rare in the group of the 45S5 bioglass), fatty infiltrate (not detectable in all groups), and necrosis (not detectable in all groups).

The irritancy score was calculated based on the scoring results. The calculation showed that the ICIE16 bioglass had an average treatment irritancy of 18.5 at day 10 post implantation, and an overall irritancy score of 1.3; hence, the biomaterial was considered non-irritant at this time point (Table V). The ICIE16-Cu bioglass had an average treatment irritancy of 12.5 at day 10 post implantation, and an overall irritancy score of 0.0; hence, the biomaterial was considered non-irritant at this time point. The ICIE16-Sr bioglass had an average treatment irritancy of 13.7 at day 10 post implantation, and an overall irritancy score of 0.0; hence, the biomaterial was considered non-irritant at this time point.

At day 30 post implantation, the treatment irritancy score of the ICIE16 bioglass had a total of 18.6, and an overall irritancy score of 2.8; hence, the biomaterial was considered non-irritant at this time point (Table V). The ICIE16-Cu bioglass had an average treatment irritancy of 17.3 at day 30 post implantation, and an overall irritancy score of 1.4; hence, the biomaterial was considered non-irritant at this time point. The ICIE16-Sr bioglass had an average treatment irritancy of 14.7 at day 30 post implantation, and an overall irritancy score of 0.0; hence, the biomaterial was considered non-irritant at this time point.

Histomorphometrical analysis of the immune response. At 10 days post implantation, ICIE16-Cu induced lower numbers of pro-inflammatory M1-macrophages (612.7±429.5 cells/mm^2) than detected in the 45S5 group, which showed the highest values for pro-inflammatory macrophages (4,167±1,015 cells/mm^2). The evaluation furthermore revealed that in the ICIE16-Sr (2,508±460.3 cells/mm^2) and ICIE16 (2,603±851.6 cells/mm^2) groups, comparable numbers of M1 macrophages were found (Figure 8). Furthermore, the number of M1 macrophages was higher in the ICIE16-Sr group compared to the ICIE16-Cu group, but only the number of M1 macrophages in the 45S5 group was significantly higher than in the ICIE16-Cu group (p<0.01). In the ICIE16 group (1,953±581.1 cells/mm^2) and the 45S5 group (1,529±961.6 cells/mm^2) the number of M2 macrophages was highest followed by the ICIE16-Sr group (919.1±701.9 cells/mm^2) and the ICIE16-Cu group (47.73±39.12 cells/mm^2), without any significant differences.

At 30 days post implantation, increasing numbers of M1 macrophages were detected in the ICIE16-Cu ICIE16-Sr and ICIE16-groups (2,091±1,820, 4,126±1,207 and 3,133±1,177 cells/mm^2, respectively). Furthermore, the number of M1 macrophages in the 45S5 group decreased from 10 to 30 days (1,648±1,278 cells/mm^2).

The number of M2 macrophages remained at a relatively low level in the of the ICIE16-Cu group (859.2±380.8 cells/mm^2). In the ICIE16-Sr (1,350±230.4 cells/mm^2), the ICIE16 (1,260±662.2 cells/mm^2) and the 45S5 (1,504±1,401 cells/mm^2) groups, comparable higher numbers of M2 macrophages were found. Thereby, only in the latter group were similar numbers of M1 and M2 macrophages detected.

Histomorphometrical analysis of the implantation bed vascularization. At 10 days post implantation, the lowest numbers of vessels were found in the ICIE16-Cu group (1,316±774 vessels/mm^2), while higher numbers were determined in the ICIE16 (2,040±1,025 vessels/mm^2), 45S5 (2,643±1,331 vessels/mm^2) and ICIE16-Sr (4,012±1,791 vessels/mm^2) groups (Figure 9).

At day 30 post implantation, the lowest vessel numbers were still found in the ICIE16-Cu group (582.5±372.9 vessels/mm^2) followed by higher numbers in the ICIE16-Sr (1,806±1,548 vessels/mm^2), ICIE16 (2,461±1,280 vessels/mm^2) and 45S5 (2,669±985.5 vessels/mm^2) groups (Figure 9). Thus, comparable

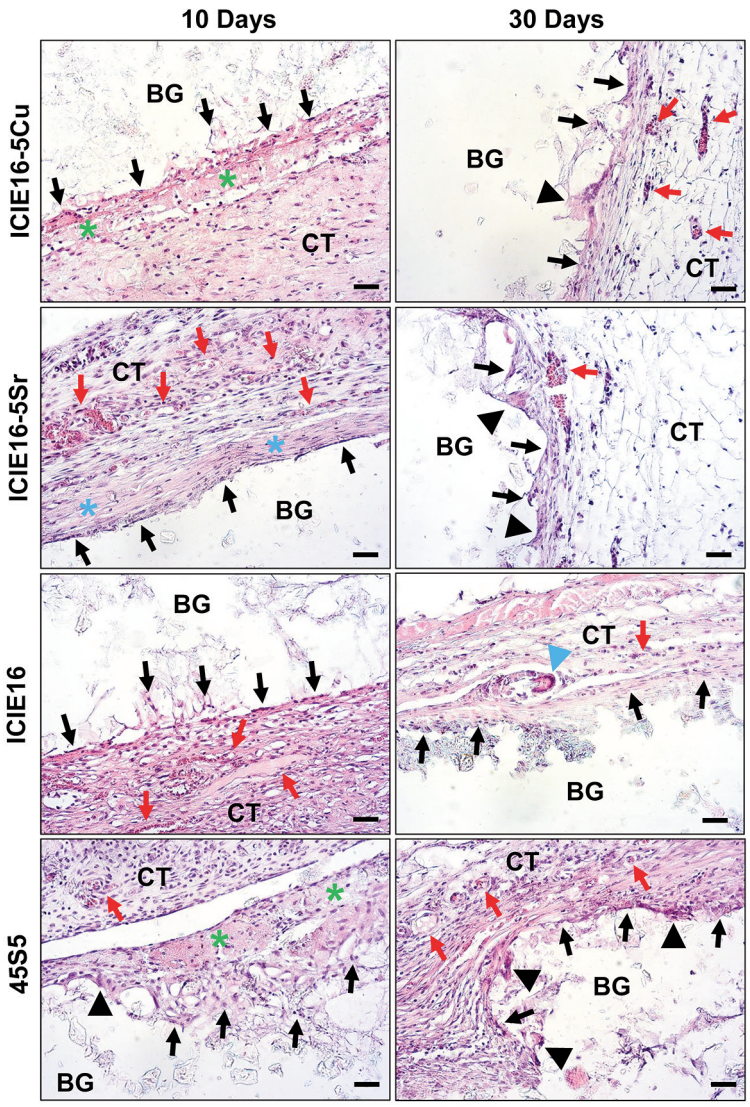

Figure 4. *Exemplary histological images showing the tissue reactions to four bioglass (BG) types within subcutaneous connective tissue (CT) at 10 days (left) and 30 days (right) after implantation. Black arrows: Mononuclear cells at the material–tissue interface; black arrowheads: multinucleated cells at the material surface; red arrows: blood vessels; green stars: fibrin network; blue arrowhead: multinucleated giant cell associated with a fragment of ICIE16 bioglass (hematoxylin and eosin staining, 20× magnification; scale bars=20 μm).*

implantation bed vascularization was found at both study time points in all groups (Figure 9).

Discussion

It is still unknown what influence so-called therapeutic ions have on inflammatory tissue reactions that are strongly associated with tissue regeneration (34). Thus, it was supposed that their inclusion can be used to control material-triggered healing process by regulating the induction of M2 macrophages (35, 36). Interestingly, the research in this field revealed immunomodulatory characteristics of different therapeutic ions indicating they lead to the reduction of the migration of macrophages, the formation of biomaterial-associated multinucleated giant cells (MNGCs) and fibrous capsules, as well as the production of inflammatory cytokines around the implanted materials (36). It was concluded that ion addition might allow regulation of immune responses by altering the ionic microenvironment (37). The use of therapeutic ions in dental applications therefore provides many advantages compared to both purely inorganic bone substitute materials and also to organic

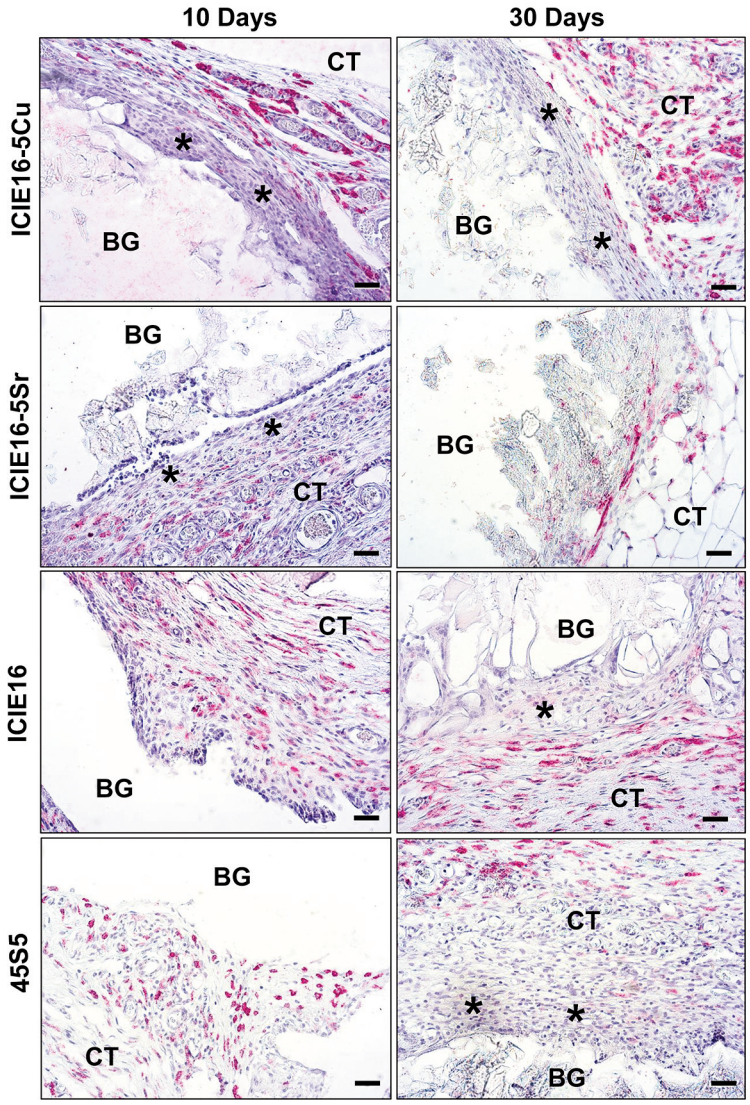

Figure 5. *Exemplary histological images showing CD163-positive M2 macrophages (red staining) within the subcutaneous connective tissue (CT) at 10 days (left) and 30 days (right) after implantation of the four bioglass (BG) types. Stars: Cell walls at the material surface that were free of M2 macrophages (CD163 immunostaining, 20× magnification; scale bars=20 μm).*

biomolecules (*e.g.*, growth factors). Altogether, the addition of therapeutic ions to BSMs, such as bioglass, might lead to a better bone-healing process by adaption of the underlying inflammatory reactions. Thus, the present study was conducted to investigate the chemical and *in vivo* influence of doping ICIE16 bioglass with 5 wt% copper, and with 5 wt% strontium ions.

Initially, the examination of the chemical composition of the bioglass *via* EDX analysis revealed that the ion-doped bioglass exhibited peaks reflecting the normal elemental distribution of the pure bioglass material and confirmed the presence of the added ions within the respective bioglass.

To determine the release of both therapeutic ions, ICP-OES analysis was conducted. Copper and strontium ions were found to be released from ICIE16 in an increasing manner over time. Additionally, it was observed that the release of both ions consistently significantly increased with time and at every time point, a significantly higher copper release was found compared to strontium. In this context, it should be mentioned that both ions are considered microelements on the basis of their relative abundance in biological cells/tissues and physiological fluids, *i.e.*, concentration >100 mg/dl and <100 mg/dl, respectively (38, 39). High concentrations of these metals can be toxic (36, 40). In the case of the bioglass

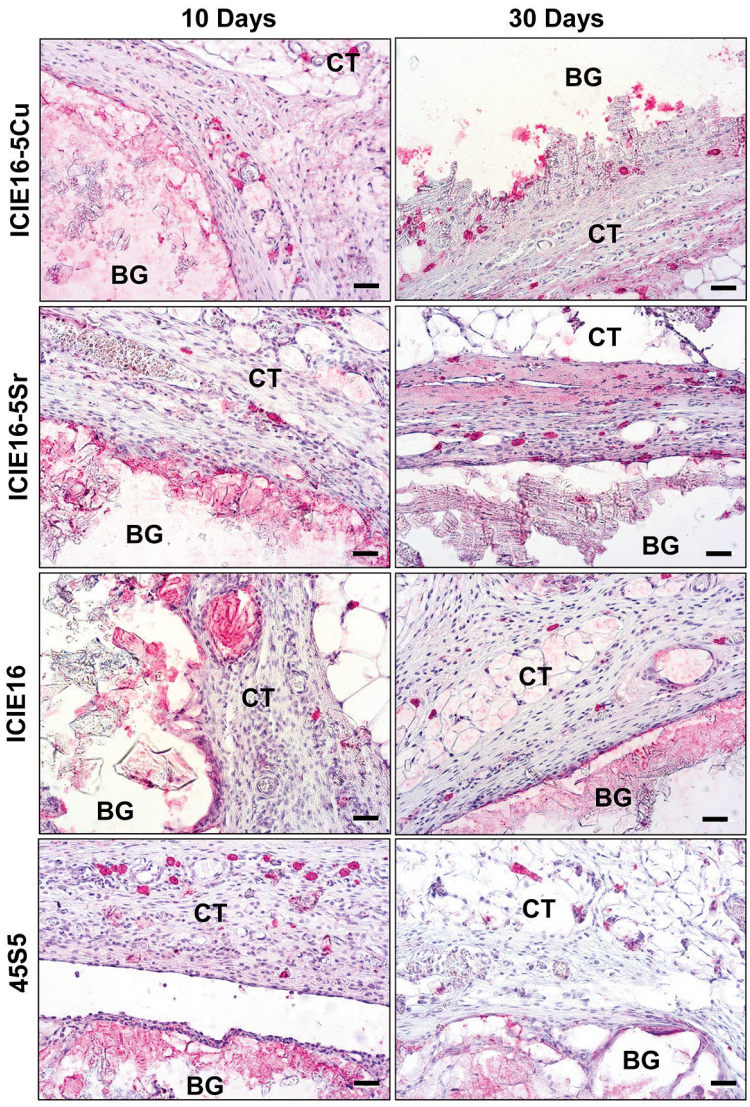

Figure 6. *Exemplary histological images showing CD11c-positive M1 macrophages (red staining) within the subcutaneous connective tissue (CT) at 10 days (left) and 30 days (right) after implantation of the four bioglass (BG) types (CD11c immunostaining, 20× magnification; scale bars=20 μm).*

materials studied here, the ion release was found to be below the above thresholds with only one exception, ICIE16-Cu at 14 days. Based on these values, an increased inflammatory reaction might be triggered by ICIE16-Cu.

The histopathological analysis showed that all bioglass types induced moderate foreign body reactions whose manifestation is usually seen in case of a broad variety of BSMs (29, 41). This reaction pattern includes formation of a granulation tissue involving mainly macrophages, biomaterial-associated MNGCs and lymphocytes, as well as blood vessels, normally starting at day 10 post implantation. Signs of (cellular) degradation were also observed beginning on day 10 post implantation, including mononuclear phagocytes within the body of the implant and the presence of biomaterial-associated MNGCs at the material surfaces. Interestingly, the intensity or cell number of the granulation tissue and thus of phagocytes decreased in all ICIE16 groups almost to slight fibrosis but not in case of the 45S5® bioglass, which suggests that the 45S5® bioglass continuously triggers a biodegrading immune reaction. This leads to the conclusion that the ICIE16 bioglass triggered the observed tissue reaction and in general underwent a lower degree of cellular biodegradation compared to that with 45S5® bioglass. Moreover, these results also showed that the addition of the therapeutic ions did not seem to influence the inflammatory tissue reaction. An explanation for the latter observation may be found in the material characteristics of both bioglass types. Thus, the larger sintering window of ICIE16 bioglass due to its composition may result in a lower tendency

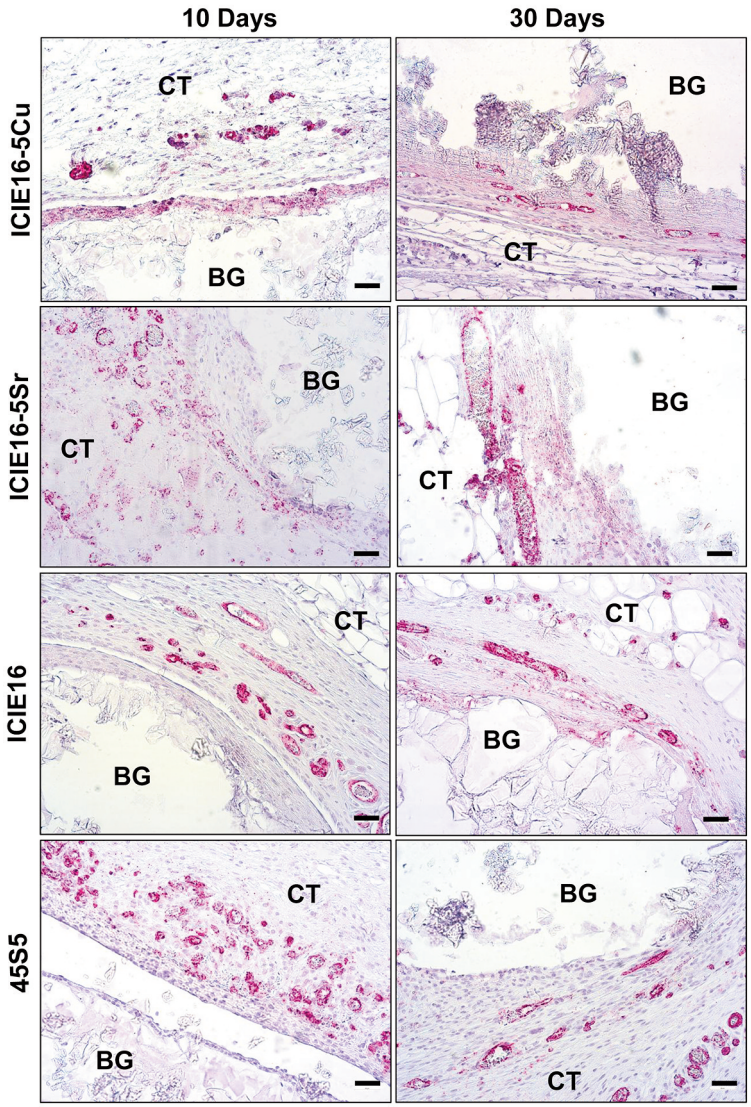

Figure 7. *Exemplary histological images showing blood vessels (red staining) within the subcutaneous connective tissue (CT) at 10 days (left) and 30 days (right) after implantation of the four bioglass (BG) types. (CD31 immunostaining; 200×, scale bars=20 μm).*

to crystallize, which may have influenced the tissue reaction at the molecular level (42, 43). In this context, it has been described that the initial binding of proteins onto biomaterial surfaces is of high importance for the overall alignment of the following tissue reaction (44). Thereby, the surface pattern of the biomaterial dictates both (a) the type of proteins bound to the surface and (b) its conformation, which will expose specific binding sites for different cell receptors and cell types and thus also dictate the foreign body cascade (45). In this context, it is conceivable that the ICIE16 bioglass induced higher expression of transforming growth factor β (TGFβ), especially isoform 1, mainly by macrophages and biomaterial-associated MNGCs (46). This finding was already shown by Hernandez-Pando *et al*., who observed that injected nitrocellulose particles initially caused biomaterial-associated MNGCs to express interleukin-1α, tumor necrosis factor α, and TGFβ (47); interestingly, TGFβ was the most persistently expressed cytokine over time and its expression was associated with extensive chronic fibrosis. An additional explanation for the observed pattern of tissue reaction might be found in the fact that the ICIE16 bioglass contains a considerably lower amount of sodium oxide; the higher sodium content of the 45S5 bioglass has been shown to induce a strong increase in local pH, which, at least in part, accounts for its dose-dependent cytotoxic effects (48).Thus, it is conceivable that the higher pH within the implantation bed of the 45S5 bioglass did not lead to fibrosis but was a trigger for faster cellular biodegradation and served as an inducer of phagocyte accumulation.

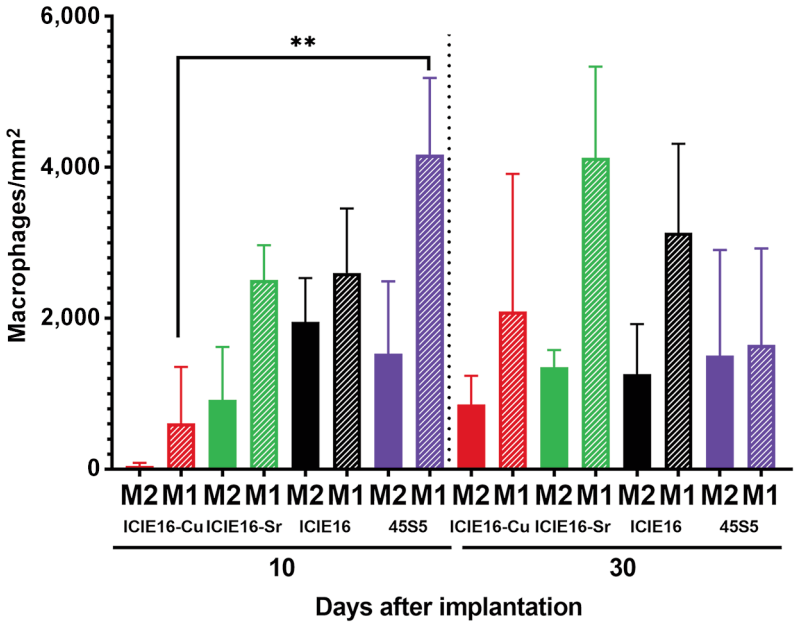

Figure 8. *Results of the histomorphometrical analysis of CD11c-positive M1 and CD163-positive M2 macrophages (cells/mm^2). ***Significantly different at p<0.001 (n=4).*

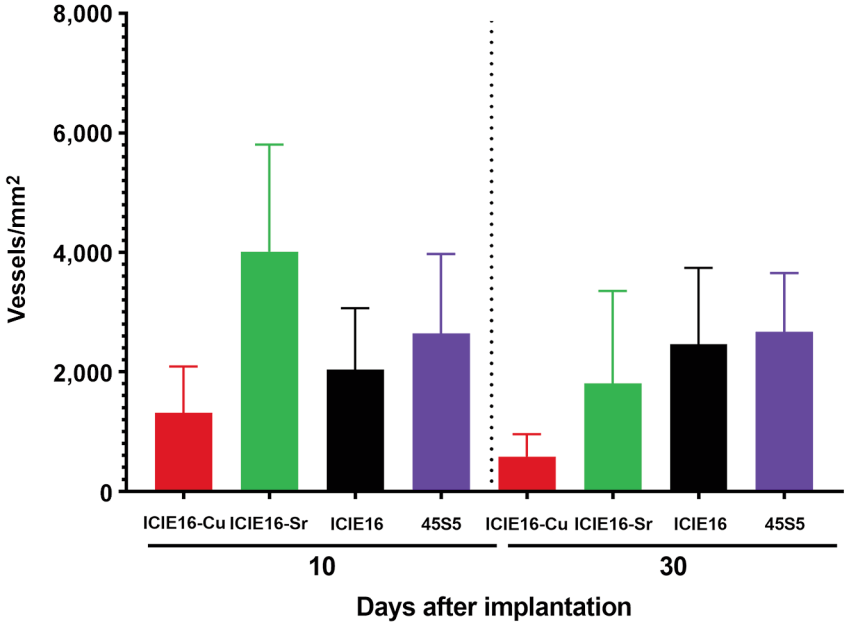

Figure 9. *Results of the histomorphometrical analysis of vessel density (vessels/mm^2) at 10 and 30 days after implantation of four bioglass types (n=4).*

However, the histopathological scoring showed that the ICIE16-based bioglass can be considered as non-irritant as it induced a slightly increased inflammatory tissue reaction involving a granulation tissue, although its appearance was similar to that observed in the control group of the 45S5 bioglass at day 10 and day 30 post implantation. Moreover, the histomorphometrical analysis revealed no significant differences between the numbers of M1 and M2 macrophages

Table IV. *Results of the evaluation of irritancy scoring of the four bioglass types. Scoring is detailed in Table II. Data are the mean scores±standard deviation.*

	ICIE16		ICIE16-Cu		ICIE16-Sr		45S5 (Control)	
Parameter	10 Days	30 Days	10 Days	30 Days	10 Days	30 Days	10 Days	30 Days
Polymorphonuclear cells	2.0±0.2	2.4±0.4	2.7±0.2	2.8±0.3	2.8±0.2	1.8±0.1	2.3±0.2	1.3±0.2
Lymphocytes	1.7±0.5	2.0±0.2	1.3±0.1	1.0±0.2	1.2±0.3	0.9±0.2	1.5±0.2	1.6±0.3
Plasma cells	0.3±0.1	0.3±0.2	0.1±0.1	0.1±0.1	0.3±0.1	0.1±0.1	0.3±0.2	0.3±0.2
Macrophages	3.0±0.0	3.0±0.0	3.0±0.0	3.0±0.0	3.0±0.0	3.0±0.0	3.0±0.0	3.0±0.0
Giant cells	1.2±0.3	0.7±0.2	0.3±0.1	0.6±0.3	0.8±0.4	0.5±0.3	1.0±0.2	1.1±0.7
Neovascularization	1.4±0.1	1.1±0.1	1.2±0.2	1.3±0.2	1.2±0.2	1.1±0.3	1.2±0.2	1.1±0.1
Fibrosis	0.8±0.2	0.8±0.3	0.8±0.2	0.8±0.2	0.9±0.3	1.0±0.0	0.1±0.1	0.2±0.1
Fatty infiltrate	0.0±0.0	0.0±0.0	0.0±0.0	0.0±0.0	0.0±0.0	0.0±0.0	0.0±0.0	0.0±0.0
Necrosis	0.0±0.0	0.0±0.0	0.0±0.0	0.0±0.0	0.0±0.0	0.0±0.0	0.0±0.0	0.0±0.0

at the different study timepoints – with only one exception for M1 macrophages for the 4S5S bioglass group compared to the ICIE16-Cu group at day 10 post implantation. This finding is also in line with the aforementioned higher phagocyte accumulation in the case of 4S5S bioglass and additionally shows its higher inflammatory potential. Interestingly, higher M1 macrophage accumulation was only detected at day 10 post implantation; this might have been the result of an increase in pH with 45S5 bioglass being restricted to the early phase after implantation. This assumption is based on the fact that is well known that an apatite layer forms at the surface of bioglass that can prevent pH shifts (14). This observation might thus be comparable with findings made after implantation of magnesium-based biomaterials (49). Recent advances in the understanding of corrosion mechanisms have shown that corrosion of magnesium continues despite the presence of an oxide layer. This layer has been shown to prevent the corrosion process marginally, but may fail to adequately protect magnesium-based implants in acidic and neutral environments, where it can corrode rapidly exposing the metal underneath to further attack. However, in our case, no influence of the addition of copper in ICIE16 was found, as the ratio of M1 and M2 macrophage numbers in the ICIE16-Cu-treated group did not significantly differ compared to the other groups.

Interestingly, the numbers of pro-inflammatory macrophages in bioglass-treated animals tended to be higher. This phenomenon is very interesting even in view of the biocompatibility of the analyzed bioglass materials. Even in the case of other BSMs, higher M1 macrophage numbers were found within their implantation beds, which is believed to be an unnatural immune response to such materials, even natural materials, such as collagen membranes, amongst others (50, 51). It was also proposed that this pro-inflammatory cell type is associated with the inflammation-based biodegradation pattern (52). In this context, various studies have revealed a dependency of the biodegradation capacity of macrophages,

Table V. *Irritancy scores and irritancy status. For each test material, the relative irritancy was calculated as: Irritancy score test material−irritancy score control material; a negative difference was assigned a score of 0. Irritancy status was assigned according to Table III.*

Time point	Study group	Overall irritancy score	Relative irritancy score	Irritant status
10 Days	ICIE16	18.5	1.3	Non-irritant
	ICIE16-Cu	12.5	0 (−4.7)	Non-irritant
	ICIE16-Sr	13.7	0 (−3.5)	Non-irritant
	45S5 (Control)	17.2	-	-
30 Days	ICIE16	18.6	2.8	Non-irritant
	ICIE16-Cu	17.3	1.4	Non-irritant
	ICIE16-Sr	14.7	0 (−1.1)	Non-irritant
	45S5 (Control)	15.8	-	-

and oxidative degradation (53). For example, it was shown that pro-inflammatory macrophages are capable of exerting oxidative stress and release lytic enzymes, such as nitric oxide and reactive oxygen species (54, 55). Moreover, high levels of reactive oxygen species were associated with high expression of pro-inflammatory cytokines in pro-inflammatory macrophages (56). Furthermore, a study by Wissing *et al*. demonstrated that lipopolysaccharide/interferon-γ treatment of macrophages led to a pro-inflammatory gene-expression profile and induced significant up-regulation of lipid peroxidation, overexpression of the oxidative genes NADPH oxidase 2 (NOX2) and nuclear factor kappa-light-chain-enhance of activated B-cells (NFκB) and increased enzymatic activity (57). Thus, the comparable numbers of M1 macrophages with the use of all bioglass types studied here may also hint at their comparable biodegradation pattern. Another interesting finding is the pattern of localization of the M1 and M2 macrophages found in all study groups. The immunohistochemical study

showed M2 macrophages remained within the surrounding granulation and connective tissues but not on the surface nor within the implant body. In contrast, pro-inflammatory M1 macrophages appeared on the surface of all implants (and also within them) starting from day 10 post implantation. These results suggest that both macrophage subtypes have different functionalities within the foreign body cascade, as already suggested (58, 59). Proinflammatory cells seem to engage in cell-mediated resorption, while anti-inflammatory cells seem to be more involved in the regeneration of the surrounding tissue – even in the time frame of the present study. However, no significant differences between the M1 and M2 macrophage subtypes were found, leading to the conclusion that all the bioglass types analyzed are biocompatible as overall, they induced balanced numbers of M1 and M2 macrophages.

Even though copper has been reported to have angiogenetic potential (60-62), no significant differences were observed in the vascularization of the implantation bed. Contradicting the *in vitro*-based predications of the angiogenetic potential of copper (26, 63), neither ICIE16-Cu nor ICIE16-Sr enhanced implant vascularization in this study.

Altogether, neither of these therapeutic ions had any biological influence on the immune response or the vascularization pattern. This result is surprising as both ions have been described to influence both molecular cascades but are in line with another *in vivo* study including an analysis of silicate-based copper-doping that also showed no influence and, more importantly, the materials in fact hindered the regeneration process (62, 64).

One limitation of this study was the short-term *in vivo* experiment. As bone regeneration occurs over a longer time period, further studies within the bony microenvironment have to be conducted in order to verify the osteogenic potential of these ion-doped bioactive glass materials. A further *in vivo* trial using bone implantation models may show another tissue reactivity of the analyzed materials. Another point to consider is that the *in vitro* investigation of ion-release in SBF can only be seen as a limited result compared to the ion-release *in vivo*. That is because SBF differs from body fluids in the following aspects: i) body fluid is a dynamic system while the ion-release measurement was conducted in a static environment; ii) body fluids are 'open' systems, which means that their components are constantly replaced/renewed whereas SBF was not changed during the analysis; and iii) SBF does not include all the components of body fluids (*e.g.*, proteins, enzymes, and ions). Thus, an *in vivo* analysis of ion release can provide more insights into the concentrations of the ions within the surrounding tissue and the overall dissolution behavior.

Another analysis method that could provide further understanding is the quantitative measurement of the nanoscale build-up of apatite and whether a correlation exists with histomorphometrical results.

Overall, the studied bioactive glass materials seemed to be biocompatible, with an acceptable foreign body reaction that is typical of synthetic BSMs. Finally, and in contradiction to published *in vitro* evaluations, copper- and strontium-doping did not significantly influence macrophage polarization, nor vascularization.

Conflicts of Interest

The Authors declare no conflicts of interest.

Authors' Contributions

Conceptualization: FS and MB; methodology: SN, SS, OG, DR, FS and MB; software: OG, FS and MB; validation: SA, FS and MB; formal analysis: AM, MR, SN, SS, FS and MB; investigation: SA, AM, YR, BC, OG, FS and MB; resources: SN, SS, OG, FS and MB; data curation: SN, SS, MR, OG, FS and MB; writing—original draft preparation: SA, SN, SS, OG, DR, FS and MB; writing—review and editing: SA, SN, FS and MB; visualization: SA, FS and MB; supervision: SN, FS and MB; project administration: SN, FS and MB; funding acquisition: SN and MB. All Authors read and agreed to the published version of the article.

References

1 Perić Kačarević Ž, Rider P, Alkildani S, Retnasingh S, Pejakić M, Schnettler R, Gosau M, Smeets R, Jung O and Barbeck M: An introduction to bone tissue engineering. Int J Artif Organs *43(2)*: 69-86, 2020. PMID: 31544576. DOI: 10.1177/0391398819876286

2 Ribas R, Schatkoski V, Montanheiro T, De menezes B, Stegemann C, Leite D and Thim G: Current advances in bone tissue engineering concerning ceramic and bioglass scaffolds: A review. Ceramics International *45(17)*: 21051-21061, 2019. DOI: 10.1016/j.ceramint.2019.07.096

3 Hench LL: The story of Bioglass. J Mater Sci Mater Med *17(11)*: 967-978, 2006. PMID: 17122907. DOI: 10.1007/s10856-006-0432-z

4 Chacko NL, Abraham S, Rao HN, Sridhar N, Moon N and Barde DH: A Clinical and radiographic evaluation of periodontal regenerative potential of PerioGlas®: a synthetic, resorbable material in treating periodontal infrabony defects. J Int Oral Health *6(3)*: 20-26, 2014. PMID: 25083028.

5 Blayney AW, Bebear JP, Williams KR and Portmann M: Ceravital in ossiculoplasty: experimental studies and early clinical results. J Laryngol Otol *100(12)*: 1359-1366, 1986. PMID: 3543181. DOI: 10.1017/s0022215100101148

6 Strunz V, Bunte M and Sauer G: [Tooth roots made of Ceravital. 1 year's clinical results with a bioactive implantation material]. Dtsch Zahnarztl Z *32(11)*: 903-904, 1977. PMID: 270402.

7 Lefebvre L, Gremillard L, Chevalier J, Zenati R and Bernache-Assolant D: Sintering behaviour of 45S5 bioactive glass. Acta Biomater *4(6)*: 1894-1903, 2008. PMID: 18583208. DOI: 10.1016/j.actbio.2008.05.019

8 Chitra S, Bargavi P, Durgalakshmi D, Rajashree P and Balakumar S: Role of sintering temperature dependent crystallization of bioactive glasses on erythrocyte and cytocompatibility. Processing

and Application of Ceramics *13(1)*: 12-23, 2020. DOI: 10.2298/PAC1901012C

9 Stähli C, James-Bhasin M, Hoppe A, Boccaccini AR and Nazhat SN: Effect of ion release from Cu-doped 45S5 Bioglass® on 3D endothelial cell morphogenesis. Acta Biomater *19*: 15-22, 2015. PMID: 25770928. DOI: 10.1016/j.actbio.2015.03.009

10 Ciraldo FE, Boccardi E, Melli V, Westhauser F and Boccaccini AR: Tackling bioactive glass excessive *in vitro* bioreactivity: Preconditioning approaches for cell culture tests. Acta Biomater *75*: 3-10, 2018. PMID: 29772346. DOI: 10.1016/j.actbio.2018.05.019

11 Elgayar I, Aliev A, Boccaccini A and Hill R: Structural analysis of bioactive glasses. Journal of Non-Crystalline Solids *351(2)*: 173-183, 2019. DOI: 10.1016/J.JNONCRYSOL.2004.07.067

12 Hmood F, Goerke O and Schmidt F: Chemical composition refining of bioactive glass for better processing features, Part I. Biomedical Glasses *4(1)*: 82-94, 2021. DOI: 10.1515/BGLASS-2018-0008

13 Westhauser F, Hohenbild F, Arango-Ospina M, Schmitz SI, Wilkesmann S, Hupa L, Moghaddam A and Boccaccini AR: Bioactive glass (BG) ICIE16 shows promising osteogenic properties compared to crystallized 45S5-BG. Int J Mol Sci *21(5)*: 1639, 2020. PMID: 32121249. DOI: 10.3390/ijms21051639

14 Baino F, Hamzehlou S and Kargozar S: Bioactive glasses: Where are we and where are we going? J Funct Biomater *9(1)*: 25, 2018. PMID: 29562680. DOI: 10.3390/jfb9010025

15 Hohenbild F, Arango Ospina M, Schmitz SI, Moghaddam A, Boccaccini AR and Westhauser F: An *in vitro* evaluation of the biological and osteogenic properties of magnesium-doped bioactive glasses for application in bone tissue engineering. Int J Mol Sci *22(23)*: 12703, 2021. PMID: 34884519. DOI: 10.3390/ijms222312703

16 Nandi S, Mahato A, Kundu B and Mukherjee P: Doped Bioactive Glass Materials in Bone Regeneration. Advanced Techniques in Bone Regeneration, 2016. DOI: 10.5772/63266

17 Goh Y, Alshemary A, Akram M, Abdul kadir M and Hussain R: Bioactive Glass: An *in-vitro* comparative study of doping with nanoscale copper and silver particles. International Journal of Applied Glass Science *5(3)*: 255-266, 2021. DOI: 10.1111/ijag.12061

18 Opitz P, Besch L, Panthöfer M, Kabelitz A, Unger RE, Emmerling F, Mondeshki M and Tremel W: Insights into the *in vitro* formation of apatite from Mg-stabilized amorphous calcium carbonate. Adv Funct Mater *31*: 2007830, 2021. DOI: 10.1002/ADFM.202007830

19 Glenske K, Donkiewicz P, Köwitsch A, Milosevic-Oljaca N, Rider P, Rofall S, Franke J, Jung O, Smeets R, Schnettler R, Wenisch S and Barbeck M: Applications of metals for bone regeneration. Int J Mol Sci *19(3)*: 826, 2018. PMID: 29534546. DOI: 10.3390/ijms19030826

20 El-Rashidy AA, Roether JA, Harhaus L, Kneser U and Boccaccini AR: Regenerating bone with bioactive glass scaffolds: A review of *in vivo* studies in bone defect models. Acta Biomater *62*: 1-28, 2017. PMID: 28844964. DOI: 10.1016/j.actbio.2017.08.030

21 Anderson JM, Rodriguez A and Chang DT: Foreign body reaction to biomaterials. Semin Immunol *20(2)*: 86-100, 2008. PMID: 18162407. DOI: 10.1016/j.smim.2007.11.004

22 Sridharan R, Cameron AR, Kelly DJ, Kearney CJ and O'Brien FJ: Biomaterial based modulation of macrophage polarization: A review and suggested design principles. Materials Today *18*: 313-325, 2015. DOI: 10.1016/J.MATTOD.2015.01.019

23 Nardone V, Zonefrati R, Mavilia C, Romagnoli C, Ciuffi S, Fabbri S, Palmini G, Galli G, Tanini A and Brandi ML: *In vitro* effects of strontium on proliferation and osteoinduction of human preadipocytes. Stem Cells Int *2015*: 871863, 2015. PMID: 26240575. DOI: 10.1155/2015/871863

24 Rossi LMM, Copes RM, Dal Osto LC, Flores C, Comim FV and Premaor MO: Factors related with osteoporosis treatment in postmenopausal women. Medicine (Baltimore) *97(28)*: e11524, 2018. PMID: 29995822. DOI: 10.1097/MD.0000000000011524

25 Lowe NM, Lowe NM, Fraser WD and Jackson MJ: Is there a potential therapeutic value of copper and zinc for osteoporosis? Proc Nutr Soc *61(2)*: 181-185, 2002. PMID: 12133199. DOI: 10.1079/PNS2002154

26 Weng L, Boda SK, Teusink MJ, Shuler FD, Li X and Xie J: Binary doping of strontium and copper enhancing osteogenesis and angiogenesis of bioactive glass nanofibers while suppressing osteoclast activity. ACS Appl Mater Interfaces *9(29)*: 24484-24496, 2017. PMID: 28675029. DOI: 10.1021/acsami.7b06521

27 Malachová K, Praus P, Rybková Z and Kozák O: Antibacterial and antifungal activities of silver, copper and zinc montmorillonites. Appl Clay Sci *53*: 642-645, 2011. DOI: 10.1016/J.CLAY.2011.05.016

28 Lindner C, PrÖhl A, Abels M, LÖffler T, Batinic M, Jung O and Barbeck M: Specialized histological and histomorphometrical analytical methods for biocompatibility testing of biomaterials for maxillofacial surgery in (pre-) clinical studies. In Vivo *34(6)*: 3137-3152, 2020. PMID: 33144417. DOI: 10.21873/invivo.12148

29 Abels M, Alkildani S, Pröhl A, Xiong X, Krastev R, Korzinskas T, Stojanovic S, Jung O, Najman S and Barbeck M: The granule size mediates the *in vivo* foreign body response and the integration behavior of bone substitutes. Materials (Basel) *14(23)*: 7372, 2021. PMID: 34885527. DOI: 10.3390/ma14237372

30 Hmood FJ, Schmidt F, Goerke O and Günster J: Investigation of chemically modified ICIE16 bioactive glass, Part II. J Ceramic Sci Technol *11*: 1-9, 2020. DOI: 10.4416/JCST2019-00031

31 Kokubo T and Takadama H: How useful is SBF in predicting *in vivo* bone bioactivity? Biomaterials *27(15)*: 2907-2915, 2006. PMID: 16448693. DOI: 10.1016/j.biomaterials.2006.01.017

32 Lindner C, Alkildani S, Stojanovic S, Najman S, Jung O and Barbeck M: *In vivo* biocompatibility analysis of a novel barrier membrane based on bovine dermis-derived collagen for guided bone regeneration (GBR). Membranes (Basel) *12(4)*: 378, 2022. PMID: 35448348. DOI: 10.3390/membranes12040378

33 DIN EN ISO 10993-6:2016: Biological evaluation of medical devices, 2016. Available at: https://www.iso.org/standard/61089.html#:~:text=ISO%2010993%2D6%3A2016%20specifies,for%20use%20in%20medical%20devices.&text=%2D%20degradable%20and%2For%20absorbable%2C,be%20solid%20or%20non%2Dsolid [Last accessed on August 9, 2022]

34 O'Neill E, Awale G, Daneshmandi L, Umerah O and Lo KW: The roles of ions on bone regeneration. Drug Discov Today *23(4)*: 879-890, 2018. PMID: 29407177. DOI: 10.1016/j.drudis.2018.01.049

35 Berthon G: Is copper pro- or anti-inflammatory? A reconciling view and a novel approach for the use of copper in the control of inflammation. Agents Actions *39(3-4)*: 210-217, 1993. PMID: 8304249. DOI: 10.1007/BF01998975

36 Díez-Tercero L, Delgado LM, Bosch-Rué E and Perez RA: Evaluation of the immunomodulatory effects of cobalt, copper and magnesium ions in a pro inflammatory environment. Sci Rep *11(1)*: 11707, 2021. PMID: 34083604. DOI: 10.1038/s41598-021-91070-0

37 Batool F, Özçelik H, Stutz C, Gegout PY, Benkirane-Jessel N, Petit C and Huck O: Modulation of immune-inflammatory responses through surface modifications of biomaterials to promote bone healing and regeneration. J Tissue Eng *12*: 20417314211041428, 2021. PMID: 34721831. DOI: 10.1177/20417314211041428

38 Somarouthu S, Ohh J, Shaked J, Cunico RL, Yakatan G, Corritori S, Tami J and Foehr ED: Quantitative bioanalysis of strontium in human serum by inductively coupled plasma-mass spectrometry. Future Sci OA *1(4)*: FSO76, 2015. PMID: 28031925. DOI: 10.4155/fso.15.76

39 Kubala-Kukuś A, Banaś D, Braziewicz J, Majewska U, Pajek M, Wudarczyk-Moćko J, Antczak G, Borkowska B, Góźdź S and Smok-Kalwat J: Analysis of copper concentration in human serum by application of total reflection X-ray fluorescence method. Biol Trace Elem Res *158(1)*: 22-28, 2014. PMID: 24573405. DOI: 10.1007/s12011-013-9884-4

40 Cortizo MC and Fernández Lorenzo de Mele M: Cytotoxicity of copper ions released from metal: variation with the exposure period and concentration gradients. Biol Trace Elem Res *102(1-3)*: 129-141, 2004. PMID: 15621934. DOI: 10.1385/bter:102:1-3:129

41 Pröhl A, Batinic M, Alkildani S, Hahn M, Radenkovic M, Najman S, Jung O and Barbeck M: *In vivo* analysis of the biocompatibility and bone healing capacity of a novel bone grafting material combined with hyaluronic acid. Int J Mol Sci *22(9)*: 4818, 2021. PMID: 34062885. DOI: 10.3390/ijms22094818

42 Perić Kačarević Z, Kavehei F, Houshmand A, Franke J, Smeets R, Rimashevskiy D, Wenisch S, Schnettler R, Jung O and Barbeck M: Purification processes of xenogeneic bone substitutes and their impact on tissue reactions and regeneration. Int J Artif Organs *41(11)*: 789-800, 2018. PMID: 29707988. DOI: 10.1177/0391398818771530

43 Boccaccini AR, Chen Q, Lefebvre L, Gremillard L and Chevalier J: Sintering, crystallisation and biodegradation behaviour of Bioglass-derived glass-ceramics. Faraday Discuss *136*: 27-44; discussion 107-23, 2007. PMID: 17955801. DOI:10.1039/b616539g

44 Luttikhuizen DT, Harmsen MC and Van Luyn MJ: Cellular and molecular dynamics in the foreign body reaction. Tissue Eng *12(7)*: 1955-1970, 2006. PMID: 16889525. DOI: 10.1089/ten.2006.12.1955

45 Lee J, Byun H, Madhurakkat Perikamana SK, Lee S and Shin H: Current advances in immunomodulatory biomaterials for bone regeneration. Adv Healthc Mater *8(4)*: e1801106, 2019. PMID: 30328293. DOI: 10.1002/adhm.201801106

46 Lari R, Fleetwood AJ, Kitchener PD, Cook AD, Pavasovic D, Hertzog PJ and Hamilton JA: Macrophage lineage phenotypes and osteoclastogenesis—complexity in the control by GM-CSF and TGF-beta. Bone *40(2)*: 323-336, 2007. PMID: 17055352. DOI: 10.1016/j.bone.2006.09.003

47 Hernandez-Pando R, Bornstein QL, Aguilar Leon D, Orozco EH, Madrigal VK and Martinez Cordero E: Inflammatory cytokine production by immunological and foreign body multinucleated giant cells. Immunology *100(3)*: 352-358, 2000. PMID: 10929057. DOI: 10.1046/j.1365-2567.2000.00025.x

48 Rizwan M, Hamdi M and Basirun WJ: Bioglass® 45S5-based composites for bone tissue engineering and functional applications. J Biomed Mater Res A *105(11)*: 3197-3223, 2017. PMID: 28686004. DOI: 10.1002/jbm.a.36156

49 Jung O, Hesse B, Stojanovic S, Seim C, Weitkamp T, Batinic M, Goerke O, Kačarević ŽP, Rider P, Najman S and Barbeck M: Biocompatibility analyses of HF-passivated magnesium screws for guided bone regeneration (GBR). Int J Mol Sci *22(22)*: 12567, 2021. PMID: 34830451. DOI: 10.3390/ijms222212567

50 Kapogianni E, Alkildani S, Radenkovic M, Xiong X, Krastev R, Stöwe I, Bielenstein J, Jung O, Najman S, Barbeck M and Rothamel D: The early fragmentation of a bovine dermis-derived collagen barrier membrane contributes to transmembraneous vascularization-a possible paradigm shift for guided bone regeneration. Membranes (Basel) *11(3)*: 185, 2021. PMID: 33803205. DOI: 10.3390/membranes11030185

51 Radenković M, Alkildani S, Stoewe I, Bielenstein J, Sundag B, Bellmann O, Jung O, Najman S, Stojanović S and Barbeck M: Comparative *in vivo* analysis of the integration behavior and immune response of collagen-based dental barrier membranes for guided bone regeneration (GBR). Membranes (Basel) *11(9)*: 712, 2021. PMID: 34564529. DOI: 10.3390/membranes11090712

52 Yunna C, Mengru H, Lei W and Weidong C: Macrophage M1/M2 polarization. Eur J Pharmacol *877*: 173090, 2020. PMID: 32234529. DOI: 10.1016/j.ejphar.2020.173090

53 Virág L, Jaén RI, Regdon Z, Boscá L and Prieto P: Self-defense of macrophages against oxidative injury: Fighting for their own survival. Redox Biol *26*: 101261, 2019. PMID: 31279985. DOI: 10.1016/j.redox.2019.101261

54 Groemping Y, Lapouge K, Smerdon SJ and Rittinger K: Molecular basis of phosphorylation-induced activation of the NADPH oxidase. Cell *113(3)*: 343-355, 2003. PMID: 12732142. DOI: 10.1016/s0092-8674(03)00314-3

55 Tan HY, Wang N, Li S, Hong M, Wang X and Feng Y: The reactive oxygen species in macrophage polarization: reflecting its dual role in progression and treatment of human diseases. Oxid Med Cell Longev *2016*: 2795090, 2016. PMID: 27143992. DOI: 10.1155/2016/2795090

56 Song MG, Ryoo IG, Choi HY, Choi BH, Kim ST, Heo TH, Lee JY, Park PH and Kwak MK: NRF2 signaling negatively regulates phorbol-12-myristate-13-acetate (PMA)-induced differentiation of human monocytic U937 cells into pro-inflammatory macrophages. PLoS One *10(7)*: e0134235, 2015. PMID: 26222138. DOI: 10.1371/journal.pone.0134235

57 Wissing TB, Bonito V, van Haaften EE, Doeselaar M van, Brugmans MM, Janssen HM, Bouten CV and Smits AI: Macrophage-driven biomaterial degradation depends on scaffold microarchitecture. Front Bioeng Biotechnol *7*: 87, 2019. DOI: 10.3389/fbioe.2019.00087

58 Jamalpoor Z, Asgari A, Lashkari MH, Mirshafiey A and Mohsenzadegan M: Modulation of macrophage polarization for bone tissue engineering applications. Iran J Allergy Asthma Immunol *17(5)*: 398-408, 2018. PMID: 30518182.

59 Barbeck M, Schröder ML, Alkildani S, Jung O and Unger RE: Exploring the biomaterial-induced secretome: physical bone substitute characteristics influence the cytokine expression of macrophages. Int J Mol Sci *22(9)*: 4442, 2021. PMID: 33923149. DOI: 10.3390/ijms22094442

60 Huang L, Xie YH, Xiang HB, Hou YL and Yu B: Physiochemical properties of copper doped calcium sulfate *in vitro* and angiogenesis *in vivo*. Biotech Histochem *96(2)*: 117-124, 2021. PMID: 32615821. DOI: 10.1080/10520295.2020.1776392

61 Zhao S, Wang H, Zhang Y, Huang W, Rahaman MN, Liu Z, Wang D and Zhang C: Copper-doped borosilicate bioactive glass scaffolds with improved angiogenic and osteogenic capacity for repairing osseous defects. Acta Biomater *14*: 185-196, 2015. PMID: 25534470. DOI: 10.1016/j.actbio.2014.12.010

62 Lin Y, Xiao W, Bal BS and Rahaman MN: Effect of copper-doped silicate 13-93 bioactive glass scaffolds on the response of MC3T3-E1 cells *in vitro* and on bone regeneration and angiogenesis in rat calvarial defects *in vivo*. Mater Sci Eng C Mater Biol Appl *67*: 440-452, 2016. PMID: 27287141. DOI: 10.1016/j.msec.2016.05.073

63 Balasubramanian P, Salinas A, Sanchez-Salcedo S, Detsch R, Vallet-Regi M and Boccaccini A: Induction of VEGF secretion from bone marrow stromal cell line (ST-2) by the dissolution products of mesoporous silica glass particles containing CuO and SrO. Journal of Non-Crystalline Solids *500*: 217-224, 2018. DOI: 10.1016/j.jnoncrysol.2018.07.073

64 Bührer G, Rottensteiner U, Hoppe A, Detsch R, Dafinova D, Fey T, Greil P, Weis C, Beier JP, Boccacini AR, Horch RE and Arkudas A: Evaluation of *in vivo* angiogenetic effects of copper doped bioactive glass scaffolds in the AV loop model. Biomedical Glasses *2*: 111-117, 2016. DOI: 10.1515/bglass-2016-0013

Received June 28, 2022
Revised July 28, 2022
Accepted August 9, 2022